Analytical Studies of Energetic Particle Resonances in Tokamaks

André Calado Coroado

An analytical method is developed for studying resonant interactions between fusion-born alpha particles and TAEs (Toroidicity-induced Alfvén Eigenmodes) for the 15 MA baseline scenario of ITER (International Thermonuclear Experimental Reactor). Building over lowest-order predictions for the orbital properties of resonant particles, these are found to disagree with numerical data, thus highlighting the need for a more advanced approach. This requires taking into account the drift-velocity terms in the resonance condition in order to understand numerical results. Analytical models for local magnetic equilibria and passing orbits are then derived, yielding accurate results for the shape of the magnetic flux surfaces and the particle's orbit. The particle's transit frequencies are then analytically derived, showing good agreement with values obtained from numerical integration of the orbits. The analytical model for the resonance condition is afterwards used to obtain approximated predictions for the orbital properties of the particles in resonance with the TAEs.

I. TAE/fusion-born α-particles resonance

Ensuring α-particle confinement in a tokamak is a mandatory condition to keep the plasma at the high temperatures needed for the fusion reaction to occur in a self-sustained way. This is raising major concern regarding ITER operation, since it is intended to reach the burning-plasma regime in order to show the viability of nuclear fusion reactors for energy production [1]. However, shear-Alfvén wave instabilities may lead to an increase of α-particle radial transport, thus destroying the α-particle confinement. An MHD approach can be used to describe shear-Alfvén waves if their characteristic length scale L is much larger than the ion Larmor radius ρ_i and mean-free path λ_i ($L \gg \rho_i, \lambda_i$), their frequency ω is much smaller than the ion cyclotron frequency Ω_i ($\omega \ll \Omega_i$), all bulk-plasma species are locally Maxwellian and all other finite Larmor radius effects are negligible. Under these conditions, the shear-Alfvén waves dispersion relation [2] is given by

$$\omega = k_{||} v_A, \tag{1}$$

where $k_{||}$ is the parallel component of the wave vector and $v_A = \frac{B}{\sqrt{\mu_0 \rho}}$ stands for the Alfvén speed, B being the magnetic-field magnitude and ρ the plasma mass density. Since fusion-born α-particles move with velocities of the order of the Alfvén speed, wave-particle resonant interactions arise. This may lead to an energy transfer from α-particles to Alfvén waves, thus making them grow unstable, which threatens α-particle confinement. Alfvén waves propagating in the plasma following the dispersion relation in (1) with finite $\frac{d\omega}{dr}$ are part of the Alfvén continuum. Since the waves damping rate satisfies $\gamma \propto \frac{d\omega}{dr}$ [2], modes from the Alfvén continuum are strongly damped, thus being harmless to α-particle confinement. However, due to toroidicity effects, wave coupling between the modes of the Alfvén continuum occurs at specific frequencies, thus giving rise to frequency gaps where weakly damped Alfvén Eigenmodes (AEs) arise [2]. When driven unstable, these gap modes may lead to an increase in α-particle radial transport. First order mode coupling $\nu = 1$ relates with Toroidicity-induced Alfvén Eigenmodes (TAEs), which arise from coupling between two counter-propagating poloidal harmonics m and $m+1$ with the same toroidal mode number n (where $m = n$). TAEs are centered around rational flux surfaces whose safety factor q is stated in terms of n and m as

$$nq = m + \frac{1}{2}. \tag{2}$$

Therefore, the TAE's radial location is set by the safety-factor radial profile. Moreover, the central gap frequency [2] is given by

$$\omega = \frac{v_A}{2Rq}, \tag{3}$$

where R is the distance measured from the torus axis to the point of interest, with the TAE's frequency being close to it.

II. Wave-particle energy-exchange

The energy-exchange between TAEs and α-particles was derived by Porcelli [3], starting from the force balance equation and evaluating the work performed by the perturbed electric field on the particle. In this process, a few assumptions have been made. To begin with, the guiding center motion approach was taken, since $\frac{\omega}{\Omega_i} \ll 1$ and $\frac{\rho_i}{L} \ll 1$ hold. The Vlasov kinetic equation gives the time evolution of the distribution function $f = F + f^{(1)}$, with F the equilibrium distribution function and $f^{(1)}$ the perturbed part satisfying $\frac{f^{(1)}}{F} \ll 1$. The particle's orbit is defined by the invariants of motion P_ϕ (canonical toroidal angular momentum), E (energy) and μ (magnetic moment), as well as a signal accounting for the direction the particle is moving ($\sigma = \pm 1$). The invariants of motion are given by

$$P_\phi = Ze\Psi + mRv_{||}\frac{B_{(\phi)}}{B},$$
$$E = \frac{1}{2}m{v_{||}}^2 + y + Ze\varphi, \quad (4)$$
$$\mu = \frac{y}{B},$$

where Ze and m are respectively the particle's charge and mass, Ψ is the poloidal magnetic flux, $B_{(\phi)}$ the magnetic-field toroidal component, φ the electrostatic potential, $v_{||}$ the particle's parallel velocity and y its perpendicular energy. Perturbations are then assumed to be periodic in time and in the toroidal direction ϕ.

The energy-exchange due to energetic α-particles is then obtained as

$$\delta W_{hot} = \int d^3\vec{x}d^3\vec{p}L^{(1)^*}f^{(1)} = \delta W_1 + \delta W_2(\omega), \quad (5)$$

where $\int d^3\vec{x}d^3\vec{p}$ denotes integration over the particle's phase space ($\vec{x}$ stands for the particle's position and $\vec{p}$ refers to its momentum) and $L^{(1)^*}$ is the complex conjugate of the particle's perturbed Lagrangian given by

$$L^{(1)} = Ze\vec{A}^{(1)}.\vec{v} - Ze\varphi^{(1)} - \mu B^{(1)}, \quad (6)$$

with $\vec{v}$ the particle's velocity and $\vec{A}^{(1)}$, $\varphi^{(1)}$ and $B^{(1)}$ standing respectively for the perturbed vector potential, electrostatic potential and magnetic-field. The energy-exchange δW_{hot} in (5) can be split in two terms, one of which depends on the TAE's frequency. This is the one which gives rise to the resonant interaction, yielding

$$\delta W_2 = -\frac{2\pi^2}{Zem^2}\sum_\sigma \int dP_\phi dE d\mu\, \tau_{pt}\left(\omega\frac{\partial F}{\partial E} - n\frac{\partial F}{\partial P_\phi}\right)\sum_{p=-\infty}^{\infty}\frac{|Y_p|^2}{\omega + n\omega_{tt} + p\omega_{pt}}, \quad (7)$$

where p is an integer and Y_p are the corresponding Fourier series amplitudes, τ_{pt} is the poloidal transit time, ω_{tt} and ω_{pt} are respectively the toroidal and poloidal transit frequencies. The gradients of the distribution function taken with respect to E and P_ϕ play a key role at determining whether the particles cause damping or drive effects. When the denominator inside the sum vanishes, a singularity arises, which in turn originates a resonant interaction. Hence, the resonance condition yields

$$\omega + n\omega_{tt} + p\omega_{pt} = 0. \quad (8)$$

If periodicity is also imposed in the poloidal direction, the poloidal mode number m will appear explicitly in the resonance condition in (8). In this case, the analytical form for δW_2 will include another integer l coming from the Fourier series expansion, which relates to p via

$$p = l - m. \quad (9)$$

Moreover, the physically relevant values of l can be found to be $l = \pm 1$, so these are the ones to be used in predictions.

Escreva uma equação aqui. (

III. ITER's 15 MA baseline scenario

The ITER baseline scenario considered in this work, characterized by a 15 MA plasma current, has been at the core of recent research (check [4], [5], [6] and [7]). It is characterized by a set of magnetic-equilibrium parameters: the distance from the torus axis to the plasma magnetic axis $R_0 = 6.4055\ m$, the distance from the magnetic axis to the plasma edge $a = 1.995\ m$, the resulting inverse aspect ratio $\varepsilon = \frac{a}{R_0} = 0.31145$, the magnetic-field amplitude at the magnetic axis $B_0 = 5.2946\ T$, the corresponding Alfvén speed ${v_A}^0 = 7.0757\times10^6\ m\ s^{-1}$ and the poloidal magnetic flux at the edge $\Psi_N = 12.144\ T\ m^2\ rad^{-1}$ (normalized by 2π). It must then be noted that the poloidal magnetic flux Ψ labeling each flux surface can be normalized by Ψ_N, thus giving rise to a new radial coordinate s defined by $s^2 = \frac{\Psi}{\Psi_N}$.

Escreva uma equação aqui. (

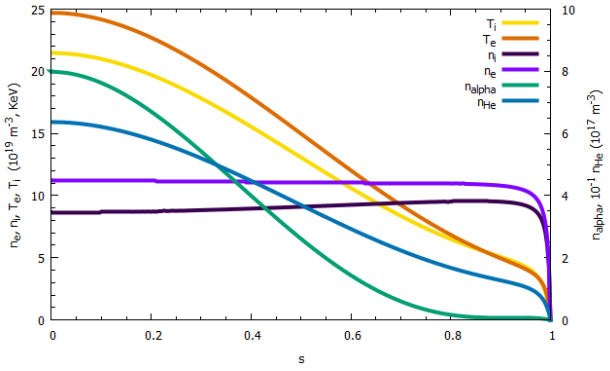

Figure 1: Radial profiles of ion and electron density and temperature, as well as α-particles and helium ash density for ITER's 15 MA baseline scenario.

This scenario is also characterized by its very low magnetic-shear, which means the radial profile of the safety factor is very flat in the plasma core. Ion and electron temperature profiles can be seen in figure 1, together with density profiles for ions, electrons, fusion-born α-particles and helium ash.

IV. Current status of AE stability predictions for ITER

A February 2015 paper by Pinches *et al* [4] explores a broad range of phenomena involving energetic ions, regarding AE stability in ITER's 15 MA baseline scenario with special concern. An analytical model is presented there to evaluate TAE stability, leading to the conclusion that unstable modes could only be observed in the outer region of the plasma $r > 0.5$ (taking r as the distance from the magnetic axis to the point of interest normalized to a). These

studies were further extended in a new article from April 2015 by Lauber [5], showing unstable TAEs in the inner half of the plasma for the same ITER scenario. Finally, new papers on TAE stability were published in June 2015 and June 2016 by Rodrigues *et al* [6] and Figueiredo *et al* [7], respectively. There, a systematic strategy was developed to assess AE stability in the presence of fusion-born α-particles, which required running the hybrid MHD/drift-kinetic code CASTOR-K [8]. This is a numerical code which follows Porcelli's aforementioned formalism [3] in order to compute δW_2 from (7). Growth rates obtained for several TAEs are depicted in figure 2.

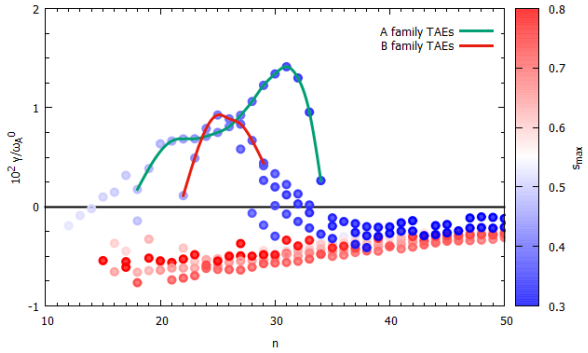

Figure 2: Growth rates of several TAEs computed by CASTOR-K plotted as a function of n and the radial location of their maximum amplitude s_{max}. The most unstable TAEs are located in the inner region $s < 0.5$ and can be seen to belong to two distinct families, corresponding to two distinct kinds of radial structures.

The highest growth rates were found for TAEs with toroidal mode number n lying in the $20 \lesssim n \lesssim 30$ range. Particularly, the $n = 31$ TAE from family A and the $n = 25$ TAE from family B prove the most unstable modes from each family, thus making them the ones requiring most attention.

V. Analytical predictions at lowest order in ε and the inverse normalized cyclotron frequency δ

The next steps will present a zeroth order derivation of the resonance condition towards determining the orbital properties of particles in resonance with the TAEs. These results will be compared with numerical data, which will reveal that higher order terms are needed to reach physically meaningful results.

Two different coordinates systems are introduced at this point: the laboratory coordinates (r, ϕ, θ), which form an orthogonal set of coordinates, with ϕ the toroidal angle and θ the poloidal angle; and the non-orthogonal field-aligned coordinates (s, ϕ, ϑ), with s defined by $s^2 = \frac{\Psi}{\Psi_N}$ and ϑ a poloidal angle such that $b^\phi = q b^\vartheta$, where b^ϕ and b^ϑ are respectively the toroidal and poloidal contravariant components of the magnetic-field unit vector $\vec{b}$. One must then obtain the poloidal transit-averaged frequencies in (8), which can be written in field-aligned coordinates as $\omega_{tt} = \langle \dot{\phi} \rangle$ and $\omega_{pt} = \langle \dot{\vartheta} \rangle$, with $\langle \ldots \rangle$ denoting an average over the poloidal transit time.

Since only leading order predictions are aimed, a simple cylindrical magnetic-equilibrium will be assumed, with no toroidicity ($\varepsilon = 0$) and centered circular flux surfaces. Under this approximation, using laboratory coordinates, the safety factor q at a given radial location r is given by

$$q(r) = \frac{ar}{R_0} \frac{B_0}{B_{(\theta)}(r)}, \tag{10}$$

where $B_{(\theta)}(r)$ is the magnetic-field poloidal component, which is a function of r but doesn't depend on θ. Taking in account that the magnetic-field components yield $\vec{B} = (0, B_0, B_{(\theta)}(r))$ under this approximation, the contravariant components of the magnetic-field unit vector $\vec{b}$ are given by

$$b^i = \left(0, \frac{B_0/R_0}{\sqrt{{B_0}^2 + B_{(\theta)}(r)^2}}, \frac{B_{(\theta)}(r)/(ar)}{\sqrt{{B_0}^2 + B_{(\theta)}(r)^2}} \right). \tag{11}$$

It can then be seen from (11) that $b^\phi = q b^\theta$, with q given by (10). Since the field-aligned poloidal angle ϑ is defined by $b^\phi = q b^\vartheta$, one concludes that $\theta = \vartheta$ holds under this approximation. This leads to the poloidal transit frequency yielding $\omega_{pt} = \langle \dot{\vartheta} \rangle = \langle \dot{\theta} \rangle$.

On the other hand, equations (2) and (9) can be combined into

$$p = -nq + \left(l + \frac{1}{2} \right). \tag{12}$$

Using these results, the resonance condition in (8) can then be written as

$$\omega + n\langle \dot{\phi} - q\dot{\theta} \rangle + \left(l + \frac{1}{2} \right) \langle \dot{\theta} \rangle = 0. \tag{13}$$

Leading order approximations for $\dot{\phi}$ and $\dot{\theta}$ are now intended, these being the contravariant components of the particle's velocity in laboratory coordinates, $v^i = (\dot{r}, \dot{\phi}, \dot{\theta})$. Therefore, one applies the Euler-Lagrange equations to Littlejohn's Lagrangian for the particle guiding center [9], these leading to the guiding center equations of motion, from which the guiding center velocity can be calculated as

$$\vec{v} = v_{||} \vec{b} - \frac{1}{m\Omega_0} \vec{b} \times \left(\mu \vec{\nabla} B + m {v_{||}}^2 (\vec{b}.\vec{\nabla}) \vec{b} \right), \tag{14}$$

where $\Omega_0 = \frac{ZeB_0}{m}$ is the on-axis ion cyclotron frequency. This can then be normalized by the on-axis Alfvén frequency

$\omega_A{}^0 = \frac{v_A{}^0}{R_0}$, thus leading to a new dimensionless parameter $\delta \equiv \frac{\omega_A{}^0}{\Omega_0}$, yielding $\delta = 0.00436$ for ITER's $15\,MA$ baseline scenario. Since this is a small parameter, it will be neglected at this stage. The second and third terms in (14) can be rewritten so that one notices they are indeed proportional to δ, thus being neglected within this approximation. This yields, at leading order, $\vec{v} = v_{||}\vec{b}$, which allows one to write $\dot{\phi} = v_{||}b^{\phi}$ and $\dot{\theta} = v_{||}b^{\theta}$. Then, one makes use of $b^{\phi} = qb^{\theta}$ to get rid of the second term in (13). Stating the particle's parallel velocity as $v_{||} = \sigma v\sqrt{1 - \frac{\mu B}{E}}$, assuming the TAE's frequency is at zeroth order given by $\omega_0 = \frac{v_A{}^0}{2qR_0}$ and considering leading order approximations, the resonance relation can be computed as

$$1 + \left(l + \frac{1}{2}\right) 2\sigma x\sqrt{1 - \Lambda} = 0, \qquad (15)$$

where new parameters $x = \frac{v}{v_A{}^0} = \sqrt{\frac{E}{E_A{}^0}}$ and $\Lambda = \frac{\mu B_0}{E}$ have been defined.

One shall then take the two $l = \pm 1$ values separately. Assuming $\Lambda < 1$, equation (15) can be solved with respect to Λ. The corresponding resonance lines in the (x, Λ) space are plotted in figure 3.

Λ increases monotonically with x and converges to $\Lambda = 1$ as the particle's energy grows. Therefore, at zeroth order in ε, passing particles with $\Lambda > 1$ cannot take part in resonant interactions. However, only energy values lower than the fusion alphas' birth energy $E_b = 3.5\,MeV$ are of physical interest in this context. For ITER's baseline scenario with $15\,MA$, the corresponding x value yields $x_b = 1.8361$.

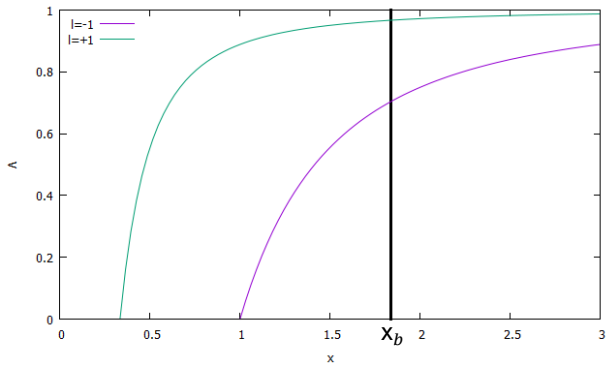

Figure 3: Resonance line in the (x, Λ) space at zeroth order for particles in resonance with a TAE, taking both $l = \pm 1$ and considering an arbitrary toroidal mode number n. Only x values on the left of $x_b = 1.8361$ are physically meaningful.

To assess the energy transfer due to each resonant orbit one must recall expression (7) for δW_2. One will take the TAE's amplitude to be concentrated in its rational flux surface, assuming that if the particle's orbit is centered around that surface and the orbit width is small, then Y_p will get a finite value, otherwise $Y_p \to 0$. After performing the transformation $(E, \mu) \to (x, \Lambda)$, the distribution function is assumed to be separable, yielding $F(P_\phi, x, \Lambda) = f_{P_\phi}(P_\phi) f_x(x) f_\Lambda(\Lambda)$. Considering that fusion-born α-particles are isotropic, one can write $f_\Lambda(\Lambda) = 1$. A slowing-down energy distribution is assumed,

$$f_x(x) = \frac{A\,H(x - x_b)}{x^3 + {x_c}^3}, \qquad (16)$$

Where A is a constant, x_c is the x value associated to a critical energy yielding $E_c = 0.6\,MeV$ for this ITER's scenario [7] and $H(x - x_b)$ is the Heaviside function. The expression for δW_2 is then simplified by taking advantage of the fact that $\omega \frac{\partial F}{\partial E} \ll n \frac{\partial F}{\partial P_\phi}$ holds for this ITER's scenario. Integrating over P_ϕ and Λ, one finds that δW_2 is given by

$$\delta W_2 \propto -n \sum_l C_l \int dx\, x^3(-2l - 1)\, \frac{H(x - x_b)}{x^3 + {x_c}^3}, \qquad (17)$$

where C_l are constant coefficients associated to each value of l. Considering only the values of physical interest, one gets $\delta W_2 > 0$ for $l = 1$, meaning the TAE is damped, while $\delta W_2 < 0$ for $l = -1$, corresponding to drive effects, which is the case of interest in this work. Taking $l = -1$, the leading order approximation for δW_2 yields

$$\delta W_2 \propto -n \int_0^{x_b} dx\, \frac{x^3}{x^3 + {x_c}^3}. \qquad (18)$$

Because $\frac{x^3}{x^3 + {x_c}^3}$ is a monotonically increasing function of x, one finds out that fusion α-particles with $x = x_b$ (i.e., $E = E_b$) are the most efficient ones at transferring energy to the TAE.

A leading order estimate for the Λ value of the maximum energy-exchange orbit is obtained by imposing $l = -1$ and $x = x_b$ in (15) and solving it with respect to Λ, which yields

$$\Lambda \cong 0.70 \qquad (19)$$

This shows that the α-particles that most efficiently drive TAEs unstable have $x = x_b$ and $\Lambda \cong 0.70$. Moreover, these lowest order predictions extend to all values of n, since the resonance condition is independent of n at leading order.

VI. Numerical results and the need for further analytical studies

CASTOR-K was used to validate these lowest-order estimates. Considering a certain TAE, CASTOR-K computes the energy exchange for different values of Λ, integrating it over the (E, P_ϕ) space. These results are plotted in figure 4, where the highest energy-exchange is

observed at $\Lambda < 0.4$ for each of the modes considered (the peak at $\Lambda \sim 0.8$ is due to numerical convergence issues). This disagrees with the leading order prediction that the most efficient particles at exchanging energy would be the ones with $x = x_b$ and $\Lambda \cong 0.70$.

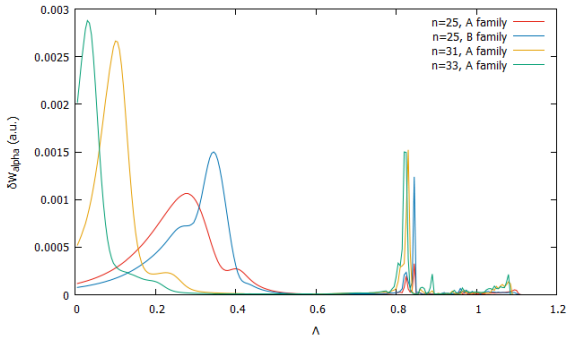

Figure 4: Energy-exchange distribution from α-particles to some TAEs ($n = 25$, $n = 31$ and $n = 33$) as a function of Λ.

Moreover, the energy transfer distribution in Λ proves different from TAE to TAE according to the value of n, which is not predicted by the leading order estimates. Therefore, higher order terms must be considered in the resonance condition in (8), which requires including the drift-velocity terms of first order in δ in (14). In order for this to be consistent, the magnetic-equilibrium must be modelled in a more accurate way too.

VII. Local magnetic-equilibrium model for analytical studies in tokamaks

Because analytical results must hold for all TAEs of interest, which have distinct radial locations, a local model will be derived for the magnetic-equilibrium in a tokamak. The magnetic-equilibrium can be specified by the poloidal magnetic flux Ψ, which must satisfy the Grad-Shafranov equation. This is usually written in (R, Z, ϕ) coordinates (with $R = R_0(1 + \varepsilon r\cos(\theta))$ and $Z = \varepsilon r \sin(\theta)$) as [10]

$$R\frac{\partial}{\partial R}\left(\frac{1}{R}\frac{\partial \Psi}{\partial R}\right) + \frac{\partial^2 \Psi}{\partial Z^2} = -\mu_0 R^2 \frac{dP}{d\Psi} - F\frac{dF}{d\Psi}, \tag{20}$$

where $F = F(\Psi)$ is the poloidal current density flux and $P = P(\Psi)$ the plasma pressure. As an analytical solution for Ψ is intended, Solovev profiles $\left(\frac{dP}{d\Psi} = const,\ F\frac{dF}{d\Psi} = const\right)$ are assumed in a local neighborhood of the flux surface of interest, the Grad-Shafranov equation thus becoming linear. The poloidal flux is then written as $\Psi = \Psi_N\, {R_0}^2\, T\, \psi$, where ψ is a dimensionless quantity and T is an arbitrary constant with inverse squared length units. Combining a particular non-homogeneous solution with a linear combination of homogeneous solutions [11] and after some algebra, ψ can be written up to terms in ε^4 as

$$\begin{aligned}\psi(r,\theta) = r^2\varepsilon^2\big(1 + K\cos(2\theta)\big) + \\ r^3\varepsilon^3(\Delta\cos(\theta) + \eta\cos(3\theta)) + r^4\varepsilon^4\left(-\tfrac{3}{32} - \right. \\ \left.\tfrac{3K}{32} + \tfrac{\Delta}{4} + \left(-\tfrac{1}{8} - \tfrac{K}{8} + \tfrac{\Delta}{4} + \tfrac{\eta}{4}\right)\cos(2\theta) + \right. \\ \left. X\cos(4\theta)\right),\end{aligned} \tag{21}$$

The parameter K is related to flux surfaces elongation, while Δ is associated to the Shafranov shift, η accounts for a triangularity-related parameter and X is related to quadrangularity.

The value of s can thus be obtained as $s(r,\theta)^2 = {R_0}^2\, T\, \psi(r,\theta)$. The magnetic-field is in turn written as

$$\vec{B} = F(\Psi)\vec{\nabla}\phi + \frac{1}{R}\vec{\nabla}\Psi\times\overrightarrow{e_\phi}. \tag{22}$$

Following (22), the magnetic field $\vec{B} = (B_{(r)}, B_{(\phi)}, B_{(\theta)})$ becomes

$$\begin{aligned}B_{(r)} = \tfrac{\varepsilon r T\Psi_N}{1+r\varepsilon\cos[\theta]}\Big(2K\sin(2\theta) + \\ \varepsilon r\,(\Delta\sin(\theta) + 3\eta\sin(3\theta)) + \varepsilon^2 r^2\Big(\Big(-\tfrac{1}{4} - \\ \tfrac{K}{4} + \tfrac{\Delta}{2} + \tfrac{\eta}{2}\Big)\sin(2\theta) + 4X\sin(4\theta)\Big)\Big), \\ B_{(\phi)} = \tfrac{R_0 B_0}{R}\Big(1 - 8\varepsilon^2 r^2\tfrac{T^2\Psi_N{}^3}{B^2}\Big(\tfrac{5+K}{4} - \\ \Delta\Big)\Big(1 + K\cos(2\theta) + \varepsilon r(\Delta\cos(\theta) + \\ \eta\cos(3\theta)) + \varepsilon^2 r^2\Big(-\tfrac{3}{32} - \tfrac{3K}{32} + \tfrac{\Delta}{4} + \Big(-\tfrac{1}{8} - \\ \tfrac{K}{8} + \tfrac{\Delta}{4} + \tfrac{\eta}{4}\Big)\cos(2\theta) + X\cos(4\theta)\Big)\Big)^{\frac{1}{2}} \\ B_{(\theta)} = \tfrac{\varepsilon r T\Psi_N}{1+r\varepsilon\cos[\theta]}\Big(2(1 + K\cos(2\theta)) + \\ 3\varepsilon r\big(\Delta\cos(\theta) + \eta\cos(3\theta)\big) + \varepsilon^2 r^2\Big(-\tfrac{3}{8} - \\ \tfrac{3K}{8} + \Delta + \Big(-\tfrac{1}{2} - \tfrac{K}{2} + \Delta + \eta\Big)\cos(2\theta) + \\ 4X\cos(4\theta)\Big)\Big),\end{aligned} \tag{23}$$

Determination of parameters (T, K, Δ, η, X) is carried out by using an accurate numerical solution of the Grad-Shafranov equation produced by the equilibrium code HELENA [12]. It provides the flux surfaces' shape for a set of radial locations $0 < s < 1$ in the poloidal plane. Then, a least squares fitting procedure is used to minimize a cost function given by the sum over all flux surface points of the squared differences between the numerical value of s^2 and the one achieved from (21) for a set of guess parameters. Figure 5 shows the parameter variation in the core of the plasma ($0.2 < s < 0.5$).

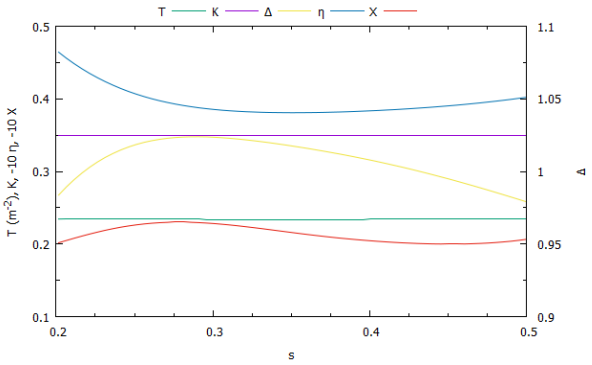

Figure 5: Radial variation of the magnetic equilibrium parameters T, K, Δ, η and X between $s \cong 0.2$ and $s \cong 0.5$ obtained from HELENA.

Other local models have been created in the past, as the one derived by Miller *et al* [13]. However, the parameters used by Miller are defined in a way that leads to transcendental combinations of trigonometric functions (for instance, equation 37 of [13]), which is much more complicated than the linear or rational combinations of trigonometric functions appearing in (23).

Following the flux function Ψ obtained in (21), an expression relating both the radial and poloidal coordinates (r, θ) along the flux surface $s = const$ is derived. Assuming truncation to fourth order in ε, $r_{surf}(\theta)$ yields

$$r_{surf}(\theta) = \frac{s}{a\sqrt{T}\sqrt{\psi_0}} - \frac{s^2\varepsilon\psi_1}{2a^2T\psi_0^2} - \frac{s^3\varepsilon^2(-5\psi_1^2+4\psi_0\psi_2)}{8a^3T^{3/2}\psi_0^{7/2}} + \frac{s^4\varepsilon^3(-2\psi_1^3+3\psi_0\psi_1\psi_2)}{2a^4T^2\psi_0^5} + \frac{7s^5\varepsilon^4(33\psi_1^4-72\psi_0\psi_1^2\psi_2+16\psi_0^2\psi_2^2)}{128a^5T^{5/2}\psi_0^{13/2}}, \quad (24)$$

where coefficients multiplying $\varepsilon^2 r^2$, $\varepsilon^3 r^3$ and $\varepsilon^4 r^4$ in expression (21) have respectively been written as

$$\begin{aligned} \psi_0 &= 1 + K\cos(2\theta), \\ \psi_1 &= \Delta\cos(\theta) + \eta\cos(3\theta), \\ \psi_2 &= \left(-\frac{3}{32} - \frac{3K}{32} + \frac{\Delta}{4} + \left(-\frac{1}{8} - \frac{K}{8} + \frac{\Delta}{4} + \frac{\eta}{4}\right)\cos(2\theta) + X\cos(4\theta)\right)\right). \end{aligned} \quad (25)$$

Using form (24), every analytically obtained flux surface can be plotted together with the corresponding numerical flux surface. The relative error can then be computed as

$$e_r = \frac{r_{analytic} - r_{numerical}}{r_{numerical}} \times 100\%. \quad (26)$$

Taking for instance the $s = 0.37075$ flux surface, plotted in figure 6, the error of the analytical surface is of the order of 0.001%, always falling shorter than 0.002%, as can be seen in figure 7. This shows that truncating the poloidal magnetic flux function at the fourth order in ε brought extremely accurate results for $s < 0.5$.

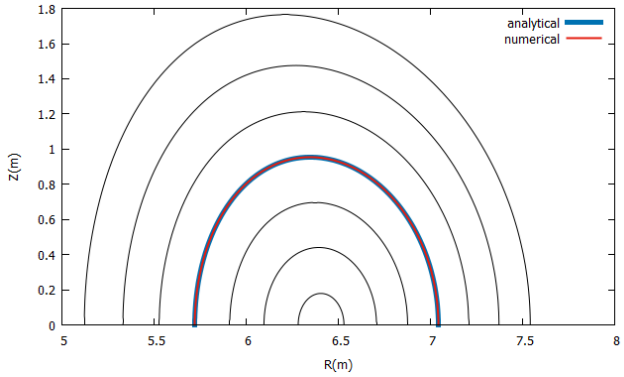

Figure 6: Analytic vs numerical magnetic flux surfaces for $s = 0.37075$, with the analytical one having been calculated up to fourth order terms. Numerical flux surfaces with different values of s are also depicted.

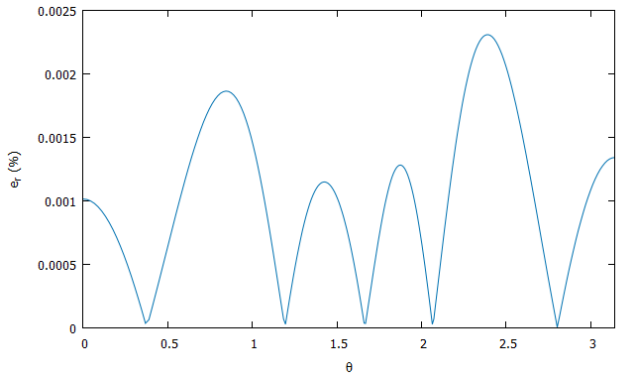

Figure 7: Relative error of the analytically obtained magnetic flux surface labeled by $s = 0.37075$.

VIII. An analytical form for charged-particles passing orbits

Poloidal transit-averaged frequencies in (8) must be written in terms of the new magnetic-field components in (23). The components of $\vec{B}$ are also dependent on the radial coordinate r, which is that associated to the particle radial location in a given point along its orbit. Therefore, all r occurrences must be replaced by the corresponding analytical form of the particle orbit in the poloidal plane, which requires solving the equation of motion for charged-particles [9]. This will be the equation for P_ϕ in (4), which can after some algebra be stated as

$$\tilde{P}_\phi = \frac{\Psi_N T}{B_0}[r^2\varepsilon^2\psi_0 + r^3\varepsilon^3\psi_1 + r^4\varepsilon^4\psi_2] + \delta\sigma x\sqrt{1 - \Lambda\frac{B}{B_0}}\frac{B_{(\phi)}}{B}(1 + \varepsilon r\cos(\theta)), \quad (27)$$

where the normalization $\tilde{P}_\phi = \frac{P_\phi}{ZeB_0R_0^2}$ has been used. Since ε and r come always together exhibiting the same exponent, one may take the radial coordinate r as the product of a

constant r_{orb} standing for the particle's average radial location and a radial coordinate $\tilde{r}\sim 1$, such that $r = r_{orb}\tilde{r}$. The ordering parameter in equation (27) will now be $\tilde{\varepsilon} = r_{orb}\varepsilon$, as εr will be replaced by $\tilde{\varepsilon}\tilde{r}$. The order of the terms involved in the orbit equation is then determined by both the small parameters $\tilde{\varepsilon}$ and δ. Assuming they are related by $\delta = \tilde{\varepsilon}^{\beta}$, with β some integer, one has

$$\beta = \frac{\log(\delta)}{\log(\varepsilon) + \log(r_{orb})}. \tag{28}$$

where $\tilde{\varepsilon} = \varepsilon r_{orb}$ was used. For the particular case under study, the orbits of α-particles in resonance with TAEs are located in the $s \in [0.2,0.5]$ range. Since $r\sim s$, this corresponds approximately to $r_{orb} \in [0.2,0.5]$. Therefore, expression (28) can be used to show that $\beta\sim 2$ comes out as a reasonable assumption within this range, the ordering condition relating δ and β thus becoming

$$\delta\sim\tilde{\varepsilon}^2. \tag{29}$$

Returning to the orbit equation in (27), one notes that a series expansion in only one variable would be easier to deal with than a two-parameter series expansion. This requires explicitly eliminating δ from (27) by introducing

$$\gamma = \frac{x\delta B_0}{2\tilde{\varepsilon}^2\Psi_N T}\sim 1. \tag{30}$$

Using this new parameter and expanding equation (27) in power series of $\tilde{\varepsilon}$, one becomes able to express it as

$$\begin{aligned}
&\frac{U^2}{2} = G\tilde{\varepsilon}\tilde{r} + \left(W\tilde{\varepsilon}^2 + \frac{\psi_0}{2}\right)\tilde{r}^2 + \frac{\psi_1\tilde{\varepsilon}}{2}\tilde{r}^3 + \frac{\psi_2\tilde{\varepsilon}^2}{2}\tilde{r}^4,\\
&\frac{U^2}{2} = \bar{P}_\phi - \sigma\gamma\sqrt{1-\Lambda},\\
&G = \sigma\gamma\frac{1-\frac{\Lambda}{2}}{\sqrt{1-\Lambda}}\cos(\theta),\\
&W = \sigma\gamma(j + h\cos(2\theta)),\\
&j = -\frac{{B_0}^2\Lambda^2 + 8{\Psi_N}^2T^2(\Lambda-1)(2(\Lambda-2)K^2 + \Lambda K + (7-4\Delta)\Lambda - 4)}{16{B_0}^2(1-\Lambda)^{3/2}},\\
&h = -\frac{{B_0}^2\Lambda^2 + 8K{\Psi_N}^2T^2(\Lambda-1)\left((9+K-4\Delta)\Lambda - 8\right)}{16{B_0}^2(1-\Lambda)^{3/2}}.
\end{aligned} \tag{31}$$

Before proceeding, it must be highlighted that this only holds for passing particles, for which $\Lambda\frac{B}{B_0} < 1$ everywhere. Otherwise, imaginary terms would appear and equation (31) would not be valid, this being the case if trapped orbits were considered. Nonetheless, only low Λ values are concerned in this work, so equation (31) can be used.

After analytically solving the polynomial equation in (31), the resulting solution will be expanded in power series of $\tilde{\varepsilon}$ up to second order terms. This is consistent with the ordering in (29) since only first order in δ terms will be kept in the resonance condition. The resulting terms are afterwards simplified, yielding

$$\begin{aligned}
\tilde{r}(\theta) = {}& \frac{U}{{\psi_0}^{\frac{1}{2}}} - \frac{2G\psi_0 + U^2\psi_1}{2{\psi_0}^2}\tilde{\varepsilon} + \\
& \frac{4G^2{\psi_0}^2 - 4U^4\psi_0\psi_2 - 8WU^2{\psi_0}^2 + 12GU^2\psi_0\psi_1 + 5U^4{\psi_1}^2}{8U{\psi_0}^{7/2}}\tilde{\varepsilon}^2,
\end{aligned} \tag{32}$$

Analytical orbits of passing particles can then be plotted by following expression (32). One chooses to plot the orbit obtained by CASTOR-K for the particles which prove the most efficient at transferring energy to the $n = 31$ TAE from the A family. This requires using the $(\tilde{P}_\phi, E, \Lambda)$ set given by CASTOR-K, as well as equilibrium parameters for the particle's average radial location. This is obtained from the TAE's safety-factor q given by (2), since the orbit is assumed to drift around the mode's rational flux surface, at $s = 0.37208$. The analytical orbit $r(\theta)$ for particles with $\tilde{P}_\phi = 0.0155859375$, $x = 1.80736$ and $\Lambda = 0.102$ is plotted in figure 8.

Similarly to what had been previously noticed for the analytical magnetic flux surfaces, the analytical and numerical orbits show good agreement. Indeed, computing the relative error by means of (26), this is found to be of the order of 0.1%, as can be observed in figure 9.

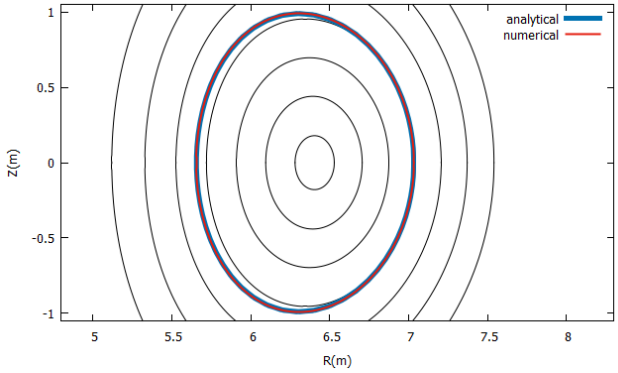

Figure 8: Analytical and numerical orbits projected in the poloidal cross section for passing α-particles moving around the $s = 0.37208$ magnetic flux surface. Several numerical magnetic flux surfaces are also represented.

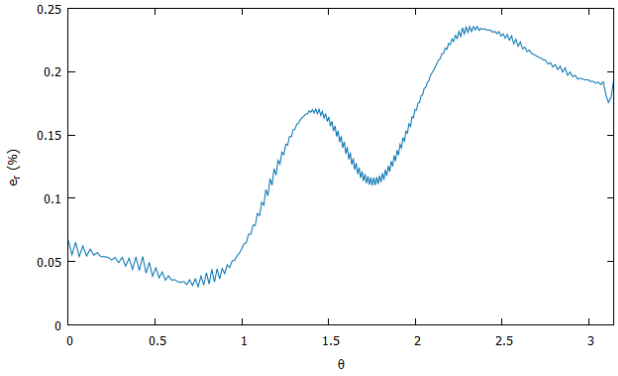

Figure 9: Relative error of the analytical orbit for passing α-particles moving around the $s = 0.37208$ flux surface.

IX. Analytical resonance condition: results and conclusions

Taking expression (14), the particle's velocity is written as

$$\begin{gathered}\vec{v} = \sigma x {v_A}^0 \sqrt{1-\Lambda\frac{B}{B_0}}\overrightarrow{\theta_1} - \\ \frac{2\tilde{\varepsilon}^2\Psi_N T\gamma}{B_0} x {v_A}^0 R_0\left[\left(1-\Lambda\frac{B}{B_0}\right)\overrightarrow{\theta_2}+\frac{\Lambda}{2B_0}\overrightarrow{\theta_3}\right], \\ \overrightarrow{\theta_1} = \vec{b}, \\ \overrightarrow{\theta_2} = \vec{b}\times\left[\left(\vec{b}.\vec{\nabla}\right)\vec{b}\right], \\ \overrightarrow{\theta_3} = \vec{b}\times\vec{\nabla}B.\end{gathered} \tag{33}$$

where the second and third terms are the ones related to drift-velocity contributions. This allows one to obtain the contravariant components of the particle's velocity in laboratory coordinates, $v^i = (\dot{r}, \dot{\phi}, \dot{\theta})$. Since the resonance condition (8) is intended in field-aligned coordinates (s, ϕ, ϑ), the transformation $(r, \phi, \theta) \rightarrow (s, \phi, \vartheta)$ must be performed.

$\dot{\vartheta}$ can be obtained from the laboratory coordinates as

$$\dot{\vartheta} = \frac{\partial\vartheta}{\partial r}\dot{r} + \frac{\partial\vartheta}{\partial\theta}\dot{\theta}. \tag{34}$$

The starting point for computing $\vartheta(r,\theta)$ will be the field-aligned coordinates definition $b^\phi = q b^\vartheta$, where b^ϑ is related to b^r and b^θ analogously to (34). Therefore, one has

$$b^\phi = q\left(\frac{\partial\vartheta}{\partial r}b^r + \frac{\partial\vartheta}{\partial\theta}b^\theta\right), \tag{35}$$

which is a local differential equation, the local value of q being set by taking the TAE's rational flux surface as reference. Solving this requires assuming some analytical form for $\vartheta(r,\theta)$, a possible choice being

$$\vartheta(r,\theta) = \sum_{n=0}^{\infty} A_n(\theta)\,\varepsilon^n r^n, \tag{36}$$

which allows one to expand (35) in power series of ε and split it into a system of differential equations for each order in ε. Solving it, one obtains

$$\begin{gathered}\vartheta(r,\theta) = A_0(\theta) + \varepsilon r A_1(\theta) + \cdots, \\ A_0(\theta) = \frac{B_0\tan^{-1}\left(\frac{(1-K)\tan(\theta)}{\sqrt{1-K^2}}\right)}{2qT\Psi_N\sqrt{1-K^2}}, \\ A_1(\theta) = \frac{B_0\left(2+3\Delta+\eta+K(2+\Delta-\eta)+2\left(\eta+K(1+\Delta+2\eta)+K^2\right)\cos(2\theta)\right)\sin(\theta)}{4(1+K)^2qT\Psi_N(1+K\cos(2\theta))},\end{gathered} \tag{37}$$

in which higher order terms are not needed.

One is then able to compute the toroidal and poloidal transit frequencies,

$$\begin{aligned}\omega_{tt} &= \langle\dot{\phi}\rangle = \frac{1}{\tau_{pt}}\oint\frac{\dot{\phi}}{\dot{\theta}}d\theta, \\ \omega_{pt} &= \langle\dot{\vartheta}\rangle = \frac{1}{\tau_{pt}}\oint\frac{\dot{\vartheta}}{\dot{\theta}}d\theta,\end{aligned} \tag{38}$$

Performing the poloidal transit-averaging in (38) will require series expansions of the integrands $\frac{\dot{\phi}}{\dot{\theta}}$ and $\frac{\dot{\vartheta}}{\dot{\theta}}$ in $\tilde{\varepsilon}$ and integrations over θ, the resulting terms then requiring some algebraic simplifications. This includes writing γ in its extended form. The fact that all γ occurrences in (31) and (32) come in terms proportional to $\tilde{\varepsilon}^2$ allows the $\tilde{\varepsilon}^2$ factors to cancel out and these terms become proportional to δ.

The resonance condition in (8) can afterwards be normalized by the on-axis Alfvén frequency, finally yielding

$$\begin{gathered}\widetilde{\omega} + n\widetilde{\omega}_{tt} + p\widetilde{\omega}_{pt} = 0, \\ \widetilde{\omega}_{tt} = \sigma x {\Lambda_1}^{1/2} + \\ \frac{\sigma x}{16{B_0}^2\Psi_N T{\Lambda_1}^3}\left[{B_0}^2\Psi_N T U^2\tilde{\varepsilon}^2\left({\Lambda_1}^{3/2}\Lambda_5\kappa_1 + 2{\Lambda_1}^{3/2}\Lambda_4\kappa_2\right) + 8{\Psi_N}^3T^3U^2\tilde{\varepsilon}^2{\Lambda_1}^{5/2}\sigma_2\right] + \\ \frac{x^2\delta}{8}\frac{B_0}{\Psi_N T}\frac{\Lambda_3\Lambda_4\kappa_1}{{\Lambda_1}^3}, \\ \widetilde{\omega}_{pt} = \frac{\sigma x {\Lambda_1}^{1/2}}{q} + \\ \frac{\sigma x}{16{B_0}^2\Psi_N Tq{\Lambda_1}^3}\left[{B_0}^2\Psi_N T U^2\tilde{\varepsilon}^2\left({\Lambda_1}^{3/2}\Lambda_5\kappa_1 + 2{\Lambda_1}^{3/2}\Lambda_4\kappa_2\right) + 8{\Psi_N}^3T^3U^2\tilde{\varepsilon}^2{\Lambda_1}^{5/2}\sigma_2\right] + \\ \frac{x^2\delta}{q}\left[\frac{\Psi_N T}{B_0}\frac{\sigma_1}{2} - \frac{B_0}{\Psi_N T}\frac{\Lambda_2\kappa_1+2\Lambda_3\kappa_2}{16\Lambda_1}\right], \\ \kappa_1 = \frac{1}{1+K}, \\ \kappa_2 = \frac{2[(K-2)\Delta+3K\eta]}{(K-1)(K+1)^2}, \\ \Lambda_1 = 1-\Lambda, \\ \Lambda_2 = 4\Lambda-\Lambda^2, \\ \Lambda_3 = 2-3\Lambda+\Lambda^2, \\ \Lambda_4 = 2-5\Lambda+3\Lambda^2, \\ \Lambda_5 = 8-20\Lambda+9\Lambda^2, \\ \sigma_1 = 4+(-1+K-4\Delta), \\ \sigma_2 = -4+(7+K-4\Delta),\end{gathered} \tag{39}$$

where all frequencies $\widetilde{\omega}$, $\widetilde{\omega}_{tt}$ and $\widetilde{\omega}_{pt}$ are normalized by the on-axis Alfvén frequency ${\omega_A}^0$.

X. Analytical predictions vs CASTOR-K results

CASTOR-K results will now be used to validate the analytical predictions for $\widetilde{\omega}_{tt}$ and $\widetilde{\omega}_{pt}$, taking the orbits which exchange most energy with the most unstable TAE. Checking numerical results from CASTOR-K for particles in resonance with the $n = 31$ TAE from family A, one has

$$\begin{aligned}\widetilde{\omega} &= 0.39537, \\ \widetilde{\omega}_{tt} &= 1.7280, \\ \widetilde{\omega}_{pt} &= 1.6863.\end{aligned} \tag{40}$$

Once the magnetic-equilibrium parameters are determined for the orbit's radial location and considering the orbit parameters given by CASTOR-K, expressions (39) can be used to obtain analytical $\widetilde{\omega}_{tt}$ and $\widetilde{\omega}_{pt}$, yielding

$$\begin{aligned}\widetilde{\omega}_{tt} &= 1.7330,\\ \widetilde{\omega}_{pt} &= 1.6916.\end{aligned} \tag{41}$$

These values are close to the numerical ones from (40), the relative errors being

$$\begin{aligned}e_{\widetilde{\omega}_{tt}} &= 0.29\%,\\ e_{\widetilde{\omega}_{pt}} &= 0.31\%.\end{aligned} \tag{42}$$

It can be noticed that these relative errors are of the same order of magnitude as the ones associated with the analytical orbit plotted in figure 8.

Next, to check the analytical resonance condition, the values of n and p must be known. Taking the $n = 31$ TAE from family A, one uses equations (2) and (12) with $m = 31$ and $l = -1$ to find $p = -32$ as the case accounting for maximum energy-exchange. An analytical estimate for the mode's frequency is provided by Nyqvist and Sharapov [14],

$$\begin{aligned}\widetilde{\omega} &= \sqrt{{\widetilde{\omega}_0}^2(1 + w\hat{\epsilon})},\\ \widetilde{\omega}_0 &= \frac{1}{2q},\\ \hat{\epsilon} &= 2\left(\varepsilon s + \frac{d\Delta_{Shaf}}{d\bar{r}}\right),\\ \Delta_{Shaf} &= \left(R_0 - \frac{R_{\theta=0} + R_{\theta=\pi}}{2}\right),\\ \bar{r} &= as,\end{aligned} \tag{43}$$

where w is an integer yielding $w = \pm 1$. The analytical estimate for $w = -1$ is found to agree with the numerical frequency of the $n = 31$ TAE. This yields

$$\widetilde{\omega} = 0.39330, \tag{44}$$

the relative error associated with it being 0.52%. Then, the resonance condition is normalized to $\widetilde{\omega}$,

$$1 + n\frac{\widetilde{\omega}_{tt}}{\widetilde{\omega}} + p\frac{\widetilde{\omega}_{pt}}{\widetilde{\omega}} = 0. \tag{45}$$

Computing the sum of the second and third terms for $n = 31$ and $p = -32$ and using analytical predictions from (41), one then obtains

$$n\frac{\widetilde{\omega}_{tt}}{\widetilde{\omega}} + p\frac{\widetilde{\omega}_{pt}}{\widetilde{\omega}} = -0.96033, \tag{46}$$

which leads to an associated relative error of 4.0%. This error is greater than that observed in the transit frequencies and the mode's normalized frequency. This is related to the fact that both terms in (46) are multiplied by n or p, which are significantly higher than the unity (~ 30).

XI. Resonance lines in the (x, Λ) space and Λ for particles with $x = x_b$ for each TAE

This analytical approach can now be used to obtain analytical resonance lines in the (x, Λ) space and compare them with numerical data. Moreover, since the highest energy transfer is theoretically predicted for α-particles at the birth energy $3.5\ MeV$, it is also interesting to obtain the value of Λ for resonant particles with $x = x_b$.

As it can be seen in figure 10, the analytically obtained resonance lines show reasonable agreement with numerical data from CASTOR-K for TAEs from family A. Even though the analytical resonance lines are displaced with respect to numerical data, these results constitute an unequivocal improvement to the lowest-order curves presented in figure 3, thus highlighting the need for the analytical formalism developed in this work.

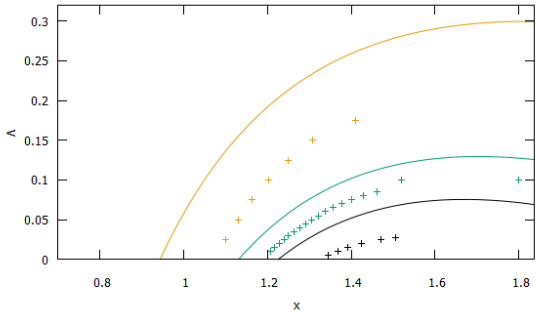

Figure 10: Analytical resonance line and CASTOR-K data in the (x, Λ) space for fusion α-particles in resonance with family A TAEs. Results for $n = 25$ (yellow), $n = 31$ (green) and $n = 33$ (black).

Further improving these results would require one to solve the limitations of the analytical method, namely assessing the radial location of the most interacting orbits and estimating the TAE's frequency.

On the other hand, obtaining the Λ values for resonant particles with $x = x_b$ yields

$$\begin{aligned}\Lambda &= 0.298, n = 25,\\ \Lambda &= 0.270, n = 26,\\ \Lambda &= 0.126, n = 31,\\ \Lambda &= 0.070, n = 33.\end{aligned} \tag{47}$$

The energy-exchange distribution is again plotted as a function of Λ in figure 11 for family A TAEs with $n = 25, 31, 33$ and the $n = 25$ TAE from family B, the corresponding values of Λ in (47) being plotted as vertical lines. It can then be seen that, apart from the $n = 33$ TAE, the analytical estimates show reasonable agreement with the distribution maxima, yielding a relative error of the order of 10%. Comparing these with the zeroth order prediction obtained in (19) for $l = -1$ shows how much this analytical method improved the analytical estimates.

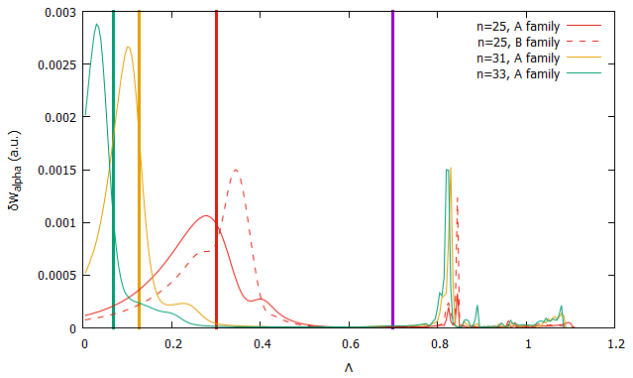

Figure 11: Energy-exchange distribution vs Λ for some TAEs ($n = 25$, $n = 31$ and $n = 33$). Vertical lines for Λ values listed in (47) are superimposed, as well as the $\Lambda = 0.70$ leading order prediction for $l = -1$ (purple).

Despite the errors in the analytical predictions of Λ being of the order of 10%, these results are far much better than the lowest order analytical estimates having been presented in section V. These analytical estimates confirm that the largest energy-exchange in the context of α-particle-TAE interactions occurs for particles with low Λ, namely $\Lambda \leq 0.4$, for the ITER scenario under consideration.

XII. Discussion and conclusions

To sum up, in this work, interesting results in distinct topics were achieved. An analytical local-equilibrium model accurate up to $(\varepsilon r)^4$ terms was obtained, thus providing a useful tool to be used in further analytical studies. Secondly, an analytical form for passing particle orbits moving in the low magnetic-shear region was derived, associated relative errors being of order 0.1%, as well as analytical forms for the corresponding poloidal and toroidal transit frequencies, with associated errors of the same order. Numerical results from CASTOR-K were used to validate the analytical transit frequencies, thus assuring the analytical method developed can be used to benchmark other gyrocenter-following codes.

Finally, a consistent analytical form was obtained for the resonance condition concerning interaction between fusion-born α-particles and the most unstable TAEs observed for ITER's $15\ MA$ baseline scenario, the corresponding relative errors lying between 1% and 10%. The results achieved provide a better agreement with numerical simulations than simple lowest-order estimates and allow one to track the essential features of the wave-particle interaction. Therefore, they lead to approximate predictions of the orbital properties of the particles in resonance with the most unstable modes.

XIII. References

[1] A. Fasoli, C. Gormenzano, H. L. Berk, B. Breizman, S. Briguglio, D. S. Darrow, N. Gorelenkov, W. W. Heidbrink, A. Jaun, S. V. Konovalov, R. Nazikian, J. M. Noterdaeme, S. Sharapov, K. Shinohara, D. Testa, K. Tobita, Y. Todo, G. Vlad and F. Zonca, Nucl. Fusion 47, S264-S284 (2007).

[2] W. W. Heidbrink, Physics of Plasmas 15, 055501 (2008).

[3] F. Porcelli, R. Stankiewicz, and W. Kerner, Phys. Plasmas 1, 470 (1994).

[4] S. D. Pinches, I. T. Chapman, P. W. Lauber, H. J. C. Oliver, S. E. Sharapov, K. Shinohara, and K. Taniet, Phys. Plasmas 22, 021807 (2015).

[5] P. Lauber, Phys. Control. Fusion 57, 054011 (2015).

[6] P. Rodrigues, A. Figueiredo, J. Ferreira, R. Coelho, F. Nabais, D. Borba, N. F. Loureiro, H. J. C. Oliver and S. E. Sharapov, Nucl. Fusion 55, 083003 (2015).

[7] A.C.A.Figueiredo, P.Rodrigues, D.Borba, R.Coelho, L.Fazendeiro, J.Ferreira, N.F.Loureiro, F.Nabais, S.D.Pinches, A.R.Polevoi and S.E.Sharapov, Nucl. Fusion 56, 076007 (2016).

[8] D. Borba and W. Kerner, Journal of Computational Physics 153, 101-138 (1999).

[9] R. G. Littlejohn, J. Plasma Phys. 29, 111 (1983).

[10] J. Wesson. *Tokamaks*, Oxford University Press Inc., New York, 2004.

[11] A. J. Cerfon and J. P. Freidberg, Phys. Plasmas 17, 032502 (2010).

[12] G. T. A. Huysmans, J. P. Goedbloed and W. W. Kerner, in Comput. Phys. 371 (World Scientific, Singapore, 1991).

[13] R. L. Miller, M. S. Chu, J. M. Greene, Y. R. Lin-Liu, and R. E. Waltz, Phys. Plasmas 5, 973 (1998).

[14] R. M. Nyqvist and S. E. Sharapov, Phys. Plasmas 19, 082517 (2012).